TU/e EINDHOVEN UNIVERSITY OF TECHNOLOGY

CFD-DEM simulation of clustering behavior in a riser

Citation for published version (APA):
Ramírez, J. G., Liu, Z., Baltussen, M. W., Buist, K. A., & Kuipers, J. A. M. (2025). CFD-DEM simulation of clustering behavior in a riser: effect of the collision model. *Powder Technology*, *453*, Article 120610. https://doi.org/10.1016/j.powtec.2025.120610

Document license:
CC BY

DOI:
10.1016/j.powtec.2025.120610

Document status and date:
Published: 15/03/2025

Document Version:
Publisher's PDF, also known as Version of Record (includes final page, issue and volume numbers)

Please check the document version of this publication:

• A submitted manuscript is the version of the article upon submission and before peer-review. There can be important differences between the submitted version and the official published version of record. People interested in the research are advised to contact the author for the final version of the publication, or visit the DOI to the publisher's website.
• The final author version and the galley proof are versions of the publication after peer review.
• The final published version features the final layout of the paper including the volume, issue and page numbers.

Link to publication

General rights
Copyright and moral rights for the publications made accessible in the public portal are retained by the authors and/or other copyright owners and it is a condition of accessing publications that users recognise and abide by the legal requirements associated with these rights.

• Users may download and print one copy of any publication from the public portal for the purpose of private study or research.
• You may not further distribute the material or use it for any profit-making activity or commercial gain
• You may freely distribute the URL identifying the publication in the public portal.

If the publication is distributed under the terms of Article 25fa of the Dutch Copyright Act, indicated by the "Taverne" license above, please follow below link for the End User Agreement:

www.tue.nl/taverne

Take down policy
If you believe that this document breaches copyright please contact us at:

openaccess@tue.nl

providing details and we will investigate your claim.

Download date: 24. Apr. 2025

Powder Technology 453 (2025) 120610

Contents lists available at ScienceDirect

Powder Technology

journal homepage: www.journals.elsevier.com/powder-technology

CFD-DEM simulation of clustering behavior in a riser - effect of the collision model

J.G. Ramírez, Z. Liu, M.W. Baltussen *, K.A. Buist, J.A.M. Kuipers

Multiphase Reactors Group, Department of Chemical Engineering & Chemistry, Eindhoven University of Technology, Eindhoven, 5600 MB, The Netherlands

GRAPHICAL ABSTRACT

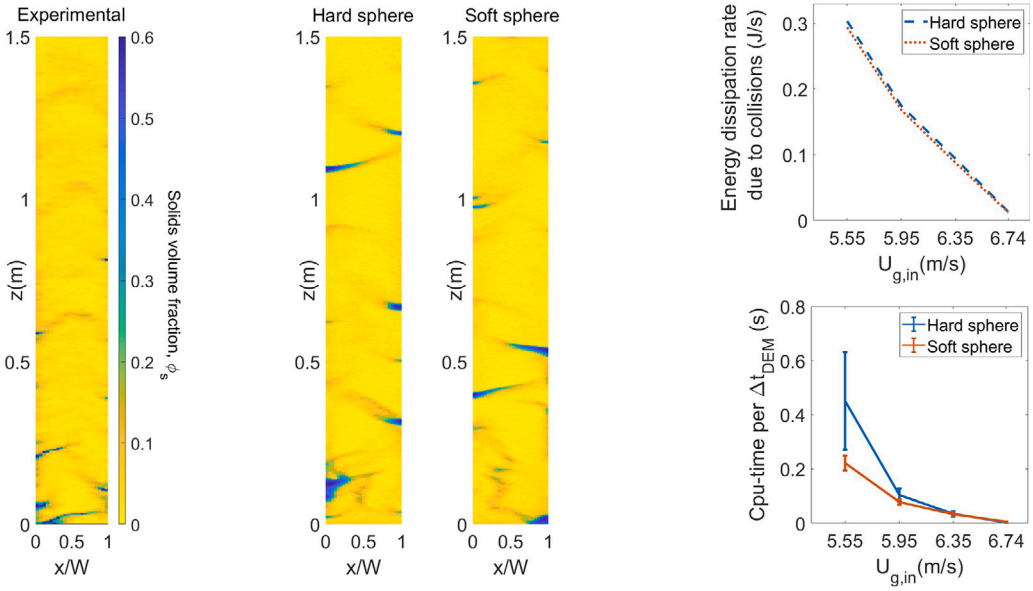

HIGHLIGHTS

- CFD-DEM riser predictions using hard and soft sphere models are compared.
- Collision frequency differences make the hard sphere model 2-6 times slower.
- Both models predict a similar energy dissipation rate due to non-ideal collisions.
- Prediction differences in solids distribution and clustering were under 7%.

ARTICLE INFO

Keywords:
CFD-DEM
Collision models
Energy dissipation

ABSTRACT

Risers play a crucial role as reactor units where important catalytic reactions occur. However, one of the drawbacks is the formation of particle clusters, which hinder the effective gas–solid interaction. This problem is primarily driven by energy dissipation due to non-ideal particle collisions. This study aims to compare the effectiveness of two common collision modeling approaches in Computational Fluid Dynamics - Discrete

* Corresponding author.
E-mail address: m.w.baltussen@tue.nl (M.W. Baltussen).

https://doi.org/10.1016/j.powtec.2025.120610
Received 21 July 2024; Received in revised form 2 December 2024; Accepted 1 January 2025
Available online 13 January 2025
0032-5910/© 2025 The Authors. Published by Elsevier B.V. This is an open access article under the CC BY license (http://creativecommons.org/licenses/by/4.0/).

Clustering
Riser

Element Model (CFD-DEM), namely hard and soft sphere model, in predicting particle clustering in a riser system in the fast fluidization regime at several superficial velocities. A pseudo-2D lab scale riser is used with dimensions 1.59 m × 0.07 m × 0.006 m. A comparison of these models is made based on the following three criteria: the cluster properties (e.g. the spatial distribution and the size of the clusters), the global variables in the riser, such as the solids volume fraction and the mass flux and finally collision variables such as collision frequency, CPU-time and dissipated energy are recorded. This study reveals significant differences in collision frequency and CPU-time between the hard and soft sphere models, especially at lower superficial gas velocities. Despite these differences, the total dissipated energy remains relatively consistent, leading to similar predictions of solids hold-up and clustering behavior. These findings hold promise for practical applications of collision models within riser systems, with the exception of scenarios approaching pneumatic transport. The simulation results show that the usage of the soft sphere model is preferred when considering dense risers, while the use of the hard sphere model can be beneficial in very dilute riser. Using this insight, an optimal CFD-DEM model can be created for optimizing reactor performance and gas–solid interaction.

1. Introduction

Risers reactors are frequently used highly important catalytic processes including the large scale production of chemical building blocks. Despite its straightforward geometric design — a duct with a single inlet at the bottom and a single outlet at the top — the gas–solid flow structure is notably complex, leading to uneven distribution of solids. This non-uniformity results in the formation of clusters, defined as localized regions with higher solids concentration [1–3]. Different authors have highlighted the downsides of these clusters on riser performance. These include increased terminal velocity due to a greater apparent diameter of the clusters relative to the particles, leading to increased solids back-mixing. Additionally, they hinder efficient gas–solid interaction and interphase transport [4–8].

CFD is a promising technique for characterizing cluster properties such as shape, size, lifetime, as well as understanding the operational factors influencing cluster formation. Cluster formation is a particle scale phenomenon, primarily driven by particle collisions, making the Discrete Element Method (DEM) a particularly suitable approach for studying and comprehending cluster dynamics. In this method, each particle is handled individually using Newton's second law of motion, allowing quantification of the impact of various variables. Several authors have explored factors such as operational conditions [3,9–11], collision parameters [1,3,11], drag and lift forces [1,11], inlet/outlet configurations [9] and equipment dimensions [1,10] on cluster properties. Notably, despite the importance of collisions in the clustering phenomena, none of the previous studies assessed the effect of collision model approaches on CFD-DEM predictions.

One approach to classify collision approaches is by distinguishing between deterministic and stochastic methods. In deterministic approaches, each particle maintains full awareness of the surrounding particles with which it can collide, usually referred to as collision partners. Collisions with these partners are computed following the time sequence governed by kinematic rules. On the other hand, stochastic approaches involve particles having only an approximate information on the current status of their neighbor partners. The order of collisions is not strictly predetermined but it is guided by probabilistic rules. Even though stochastic approaches have been used in DEM simulations to characterize clusters [3,12], it is recognized that these methods, rooted in the kinetic theory of granular flows encounter limitations when solid particles form highly packed configurations [13]. Consequently, cluster characterization with stochastic models appears feasible mainly in dilute conditions. This observation aligns with the maximum solids fraction of approximately 0.16 in the 2D simulations performed by Tanaka et al. [3] or the low number of particles per cluster found in Wang et al. [12].

The use of deterministic approaches on the other hand turned out to be robust in CFD-DEM models even when dealing with densely packed configurations such as those found in bubbling fluidized beds [1]. Within this category, two methodologies stand out: the hard sphere and the soft sphere models. In the hard sphere model, all collisions are treated as binary encounters, computed sequentially until the simulation concludes. This approach is also known as event-driven simulation. Conversely, the soft sphere approach calculates collisions based on a contact force explicitly included in Newton's second law of motion. This method integrates the collision force over a specified number of time steps along with other body forces acting on the particle, hence the soft sphere method is referred to as a time-driven simulation. Due to expected challenges in handling a highly dense system collision by collision, the soft sphere model is preferred over the hard sphere approach when quasi-static configurations are encountered. Furthermore, between those two methods, the soft sphere approach is the only one able to predict multiple particle interactions expected within such configurations. Contrarily, in dilute conditions where most collisions are binary and the free path between collisions is relatively large, the instantaneous consideration of collisions in the hard sphere approach proves more efficient than the time integration required by the soft sphere model. Within typical operating conditions a riser embodies a dual nature: it presents dilute regions, typically found in the core section of the column, and dense regions characterized by clusters primarily located near the walls. This complexity suggests that defining the best collision approach in terms of accuracy and performance is not a straightforward task. Existing literature offers insights into CFD-DEM cluster analysis that employ only one of the two models [1,9,14] or comparison attempts within a bubbling fluidized bed, —a particle system with dynamics notably distinct from those within a riser [1,15]. Although the effect of the different collision models is determined for bubbling fluidized beds, the comparison of these collision models for riser systems is to the best of the knowledge of the authors not performed. Therefore, this research distinctly focuses on providing a comprehensive comparison between these collision models within a riser.

This article initially describes the CFD-DEM model for the riser system, describing the fundamental characteristics of the collision models chosen for comparison. The results section presents first disparities in predictions generated by both collision models in terms of global variables such as solids holdup or solids flux. Subsequently, the differences are assessed in terms of collision variables such as collision frequency, energy dissipated and CPU-time. Finally, the comparison extends to clustering properties such as cluster frequency and size. The system used in this study is the pseudo-2D riser outlined in Varas et al. [14,16], leveraging experimental data reported therein for a comparative analysis between the collision models. Notably, while this work examines the same system as Carlos Varas et al. [14] and Mu et al. [9], the current study's focus lies in evaluating the collision formulations employed in the simulations, which neither of them discussed.

2. Methodology

2.1. CFD-DEM

The CFD-DEM representation used in this research, developed simultaneously by Tsuji [10] and Hoomans et al. [17], considers the gas

Nomenclature

Roman symbols

d_p	particle diameter, m
e	restitution coefficient
$\mathbf{F}_d$	drag force, N
$\mathbf{F}_{d,St}$	Stokes-Einstein drag force, N
$\mathbf{g}$	gravity, m/s^2
G_s	solids flux, kg/m^{2}s
k	spring stiffness, N/m
m_p	particle mass, kg
N_p	number of particles
P	pressure, Pa
R	particle radius, m
Re	particle Reynolds number
$\mathbf{r}_p$	position, m
$\mathbf{S}_p$	momentum source term, N/m^3
t	time, s
$\mathbf{u}_g$	gas velocity, m/s
$\mathbf{U}$	superficial slip velocity, m/s
$\mathbf{v}_p$	particle velocity, m/s
V	volume, m^3
x/W	dimensionless riser width

Greek symbols

β	inter-phase momentum transfer coefficient, kg/(m^3 s)
ε_g	gas volume fraction
μ	gas viscosity, kg/(m s)
μ_{fr}	dynamic friction coefficient
ϕ_s	solids volume fraction
ρ	density kg/m^3
$\boldsymbol{\tau}$	stress tensor, Pa

Subscripts

p	particle
g	gas
a, b	particle indices
n	normal direction
t	tangential direction
$cell$	Eulerian cell

in the riser as a continuous phase. The volume-averaged Navier–Stokes formulation and the continuity equation are used to describe the gas phase hydrodynamics (Eqs. (1) and (2), respectively).

$$\frac{\partial(\varepsilon_g\rho_g\mathbf{u}_g)}{\partial t} + \boldsymbol{\nabla}\cdot(\varepsilon_g\rho_g\mathbf{u}_g\mathbf{u}_g) = -\varepsilon_g\boldsymbol{\nabla}P - \boldsymbol{\nabla}\cdot(\varepsilon_g\boldsymbol{\tau}_g) - \mathbf{S}_p + \varepsilon_g\rho_g\mathbf{g} \tag{1}$$

$$\frac{\partial(\varepsilon_g\rho_g)}{\partial t} + \boldsymbol{\nabla}\cdot(\varepsilon_g\rho_g\mathbf{u}_g) = 0 \tag{2}$$

Where $\mathbf{S}_p$ represents the source term due to the momentum transfer between the gas and solid particles:

$$\mathbf{S}_p = \frac{1}{V_{cell}}\sum_{i=1}^{N_p}\frac{\beta V_p}{1-\varepsilon_g}(\mathbf{u}_g - \mathbf{v}_p)\delta(\mathbf{r}-\mathbf{r}_p) \tag{3}$$

The regularized Dirac delta function $\delta(\mathbf{r}-\mathbf{r}_p)$ maps the momentum exchange of each of the N_p Lagrangian particles to the relevant Eulerian velocity nodes. This same regularized function also maps the gas phase properties from the Eulerian grid to the particles position, enabling the evaluation of the drag force.

The particle motion is described using Newton's second law of motion:

$$m_p\frac{d^2\mathbf{r}_p}{dt^2} = \frac{\beta V_p}{1-\varepsilon_g}(\mathbf{u}_g - \mathbf{v}_p) - V_p\boldsymbol{\nabla}P + m_p\mathbf{g} + \underbrace{\mathbf{F_c}}_{\text{for soft sphere}} \tag{4}$$

$$\mathbf{I}_p\frac{d\boldsymbol{\omega}_p}{dt} = \mathbf{T}_p \tag{5}$$

Eq. (4) highlights that the contribution of a contact force explicitly in the Newton's second law of motion is only active when using the soft sphere approach. The principles for both approaches are described in the section below.

Since the elbow section on top of the riser does not conform to the 3D Cartesian grid, the second-order implicit Immersed Boundary Method (IBM) of Deen et al. [18] is implemented and coupled with the DEM. The strategy is described in our previous work [19].

2.2. Collision models

When a particle collides with another particle or a wall, its linear and angular momentum change due to the contact force exerted throughout the collision. In the hard sphere approach the duration of this collision force is considered notably shorter than any of the other forces acting upon the particle (right-hand side of Eq. (4)), enabling independent computation of its impact on the linear and angular momentum when the collision is detected. This method employs an impulse vector, detailed in Table 1 to alter the particle's linear and angular velocities accordingly.

The soft sphere model on the other hand approximates the contact force with a linear spring-dashpot approach (see Table 1) and includes this force in the particle's equation of motion. Termed soft sphere approach since the particles are allowed to slightly overlap when colliding, this approach uses the amount of overlap to compute

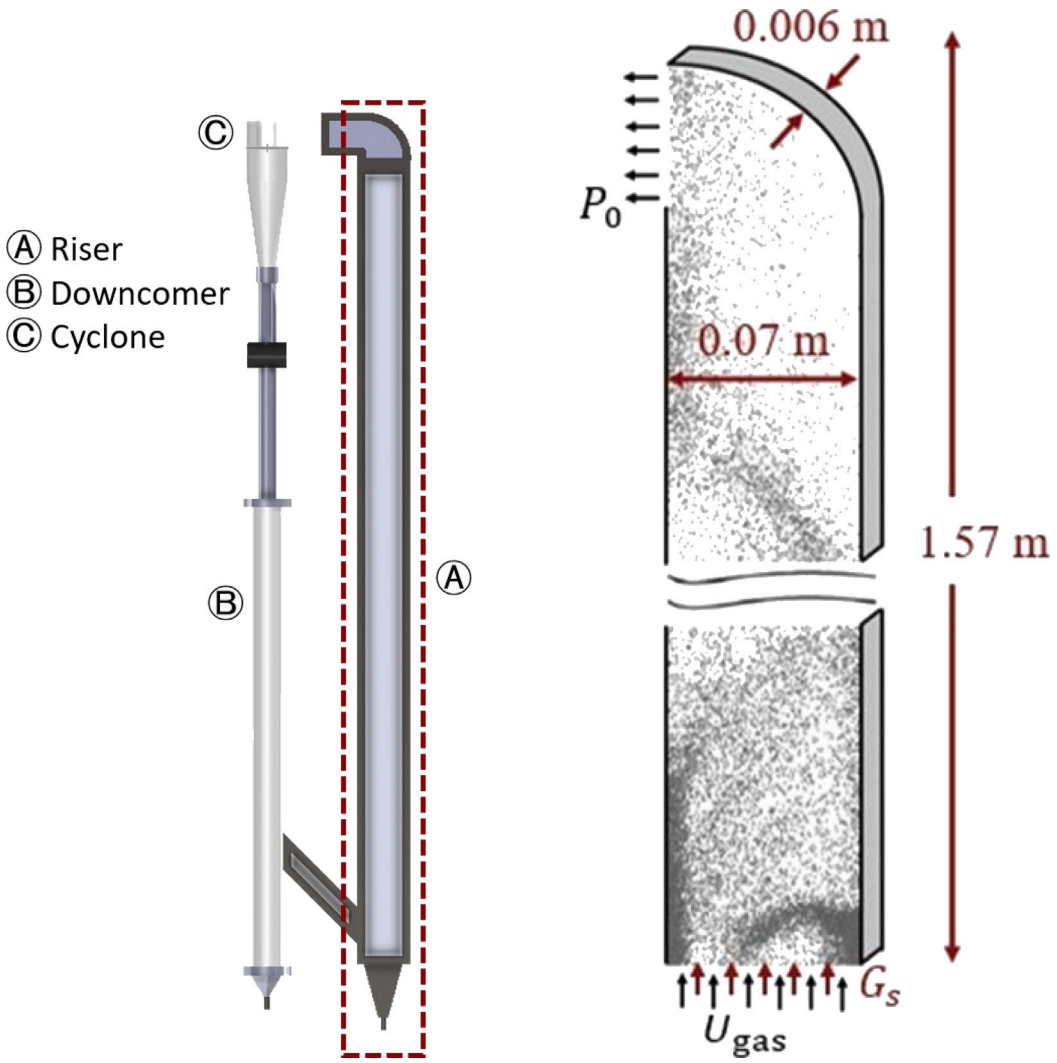

Fig. 1. Schematic representation of the riser used in this study.

the strength of the linear spring and dashpot representing the contact force. This overlapping feature provides a key advantage over the hard sphere model, allowing the soft sphere to represent particle collision with multiple other particles or walls simultaneously. The hard sphere model treats all the encounters between particles as binary collisions, persisting in modeling collisions sequentially even with densely packed particle configurations where simultaneous collisions are anticipated. One of the questions explored in subsequent sections of this article is whether this distinctive collision modeling approach yields variations in the overall predictions for the riser system.

Regarding collision detection, Eq. (6) provides the time before two objects collide in the hard sphere approach. This calculated time goes through a chronologically ordered list, comprising all potential collision times within the simulation domain. This chronological arrangement governs the time progression in this so-called event-driven simulation.

$$\delta t_{a,b} = \frac{-\mathbf{r}_{a,b}\cdot\mathbf{v}_{a,b} - \sqrt{(\mathbf{r}_{a,b}\cdot\mathbf{v}_{a,b})^2 - \mathbf{v}_{a,b}^2(-\mathbf{r}_{a,b}^2 - (R_a+R_b)^2)}}{\mathbf{v}_{a,b}^2} \tag{6}$$

In contrast, the soft sphere approach periodically checks for collision between objects at fixed time intervals (Δt_{DEM}) by evaluating their overlap. Both approaches commonly employ a neighbor list strategy to speed up collision detection, wherein potential collision partners for an object are assessed within a specific vicinity. The size of this neighbor region is a trade-off between the number of neighbors included and the frequency of neighbor list updates. Larger neighbor regions require less frequent updates but encompass numerous potential collision partners. In this study, the neighbor region constitutes a sphere surrounding each particle with a radius (r_{nb}) set at 2.3 times the radius of the particle. The neighbors inside are updated whenever a particle within the domain has moved half of the distance r_{nb}.

One significant consequence of collisions deviating from perfectly elastic behavior is energy dissipation, a factor contributing to cluster formation. Table 1 presents as well the expressions used to compute this dissipation for both collision models. A comparative analysis of this variable will be detailed in the results section.

2.3. Simulation conditions

Fig. 1 schematically shows the riser simulated in this study, as detailed in [16]. The riser (denoted as Ⓐ) is a pseudo-2D unit (0.07 m × 0.006 m × 1.57 m). It receives particles from the downcomer (Ⓑ) through a 45° lid positioned 4 cm above the riser's bottom. Particles introduced via the lid move through the riser with the air injected from its base. Upon reaching the riser's top, a cyclone (Ⓒ) separates particles from the air stream. Subsequently, particles fall back into the downcomer, which serves as a reservoir to maintain a substantial portion of the particle inventory during experiments. Additionally, air injection from the bottom of the downcomer sustains minimal fluidization conditions, ensuring a consistent particle flow from the downcomer

Table 1
Summary of collision approaches implemented in CFD-DEM model. See [20] for further details on the equations for both approaches.

Approach	Hard Sphere 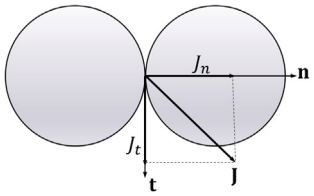	Soft Sphere 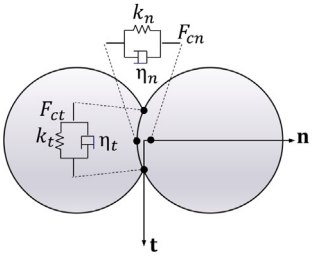
Collision formulation	Impulse vector $m(\mathbf{v}-\mathbf{v}_{,0})=\mathbf{J}$ $\frac{I}{R}(\omega-\omega_{,0})=-\mathbf{n}\times\mathbf{J}$ $\mathbf{J}=J_n\mathbf{n}+J_t\mathbf{t}$ $J_n=-(1+e_n)m_{ab}(v_{ab,0})_n$ $J_t=-\frac{2}{7}(1+e_t)m_{ab}(v_{ab,0})_t$ or in case of sliding $(\lvert J_t\rvert>\mu\lvert J_n\rvert)$ $J_t=-\mu\lvert J_n\rvert$	Linear spring dashpot $\mathbf{F_c}=F_{cn}\mathbf{n}+F_{ct}\mathbf{t}$ $F_{cn}=-k_n\delta_n-\eta_n(v_{ab})_n$ $F_{ct}=-k_t\delta_t-\eta_t(v_{ab})_t$ or in case of sliding $(\lvert F_{ct}\rvert>\mu\lvert F_{cn}\rvert)$ $F_{ct}=-\mu\lvert F_{cn}\rvert$
Integration scheme	First-order Euler	Verlet
Energy dissipation during collision	$E_{dsp}=(E_{dsp})_n+(E_{dsp})_t$ $(E_{dsp})_n=\frac{1}{2}m_{ab}(v_{ab,0})_n^2(1-e_n^2)$ $(E_{dsp})_t=\frac{1}{7}m_{ab}(v_{ab,0})_t^2(1-e_t^2)$ or in case of sliding $(E_{dsp})_t=-\mu J_n((v_{ab,0})_t-\frac{7}{4}\mu m_{ab}^{-1}J_n)$	$E_{dsp}=\int\mathbf{F_c}\cdot\mathbf{v}_{ab}dt$
$\mathbf{n}=\frac{\mathbf{r}_a-\mathbf{r}_b}{\lvert\mathbf{r}_a-\mathbf{r}_b\rvert}$	$\mathbf{t}=\frac{\mathbf{v}_{ab,0}-\mathbf{n}\cdot\mathbf{v}_{ab,0}}{\lvert\mathbf{v}_{ab,0}-\mathbf{n}\cdot\mathbf{v}_{ab,0}\rvert}$	$\mathbf{v}_{ab,0}=(\mathbf{v}_a-\mathbf{v}_b)-(R_a\boldsymbol{\omega}_a+R_b\boldsymbol{\omega}_b)\times\mathbf{n}$

to the riser via the feeding lid.

For our simulations, only the riser unit is under consideration. Thus, the interaction with the downcomer is treated as an inlet of solid particles with a constant mass flux of 32 kg/m^{2}s. In the simulations, the particles enter the riser with a prescribed constant velocity of $\{0.0, 0.0, 0.1\}$ m/s. This deviation from the real feeding condition has been proven to have a minor effect on the hydrodynamics of this riser by Mu et al. [9]. The velocity of the inlet gas, $U_{g,in}$, has a major effect on the solids distribution and clustering formation in the riser. In this study, we consider four different superficial velocities ($U_{g,in} = \{5.55, 5.95, 6.35, 6.74\}$ m/s) that range from the initial stages of particle carryover until the fast fluidization regime. Table 2 presents the relevant settings for the CFD-DEM simulations. Each simulation begins with an empty column that is gradually filled. Simulations run for 20 seconds: the first 10 s allow the system to reach a quasi-steady state in the riser, while the remaining 10 s are used to capture the desired results. Flow fields and void fraction profiles are recorded every 0.05 s.

The choice of a pseudo-2D riser facilitated experimental frame-by-frame measurements of solids distribution using a high-speed camera, as detailed in Varas et al. [16]. The same information can be obtained from the results of our simulations. Frames from both experiments and simulation serve as inputs for a clustering detection model (using a core-wake approach), enabling quantification and characterization of clusters within the riser. Further details on this clustering detection are provided in Ramírez et al. [19].

Table 2
Simulation settings.

L(m)	0.07	d_p = (mm)	0.85
H(m)	0.006	Δt_{flow}(s)	5×10^{-5}
D(m)	1.57	Δt_{DEM}(s)	5×10^{-6}
Δx(m)	2.5×10^{-3}	k_n(N/m)	1587
Δy(m)	1.25×10^{-3}	$e_{n_{p-p}}$	0.96
Δz(m)	2.5×10^{-3}	$e_{n_{p-w}}$	0.86
G_s(kg/m^2 s)	32.0	$\mu_{fr_{p-p}} = \mu_{fr_{p-w}}$	0.15
$U_{g,in}$(m/s)	5.55, 5.95, 6.35, 6.74	$e_{t_{p-p}} = e_{t_{p-w}}$	0.33
ρ_p (kg/m^3)	2500		

3. Results

3.1. Solids holdup and solids flux

Fig. 2 presents a comparison of the time-averaged solids volume fraction between experiments and CFD-DEM simulations for an intermediate gas superficial velocity. The first thing to notice is that both experiments and simulations feature the expected core-annulus flow structure. Furthermore, regarding absolute values, both collision models present a remarkable capability to predict the experimental trends along the whole riser column.

Fig. 3 extends the previous comparison by considering the different superficial gas velocities, focusing on time- and laterally-averaged solids holdup profiles. It can be seen that there is a consistent alignment

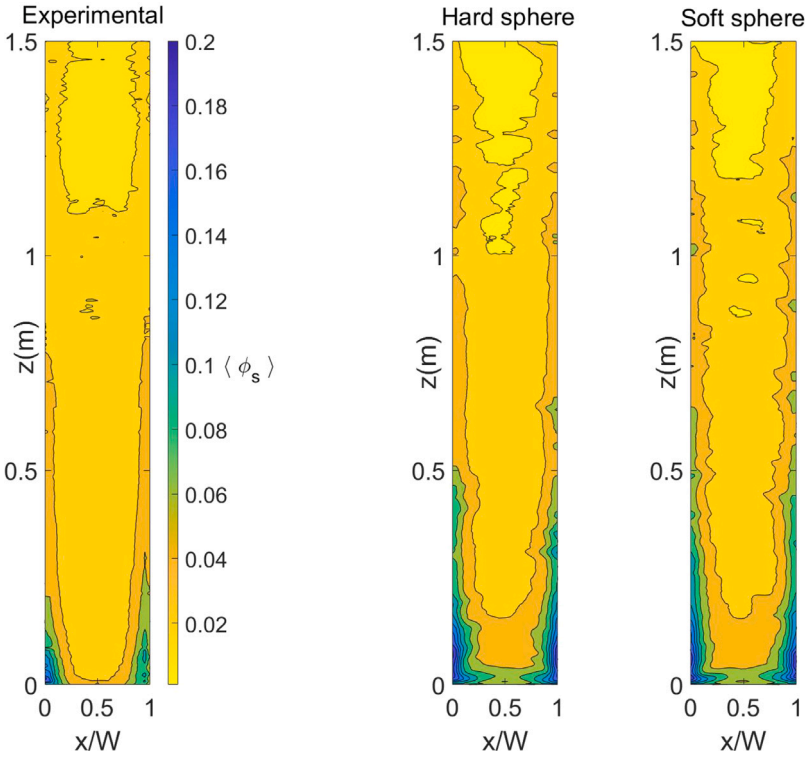

Fig. 2. Time-averaged solids volume fraction for $U_{g,in}$ = 5.95 m/s.

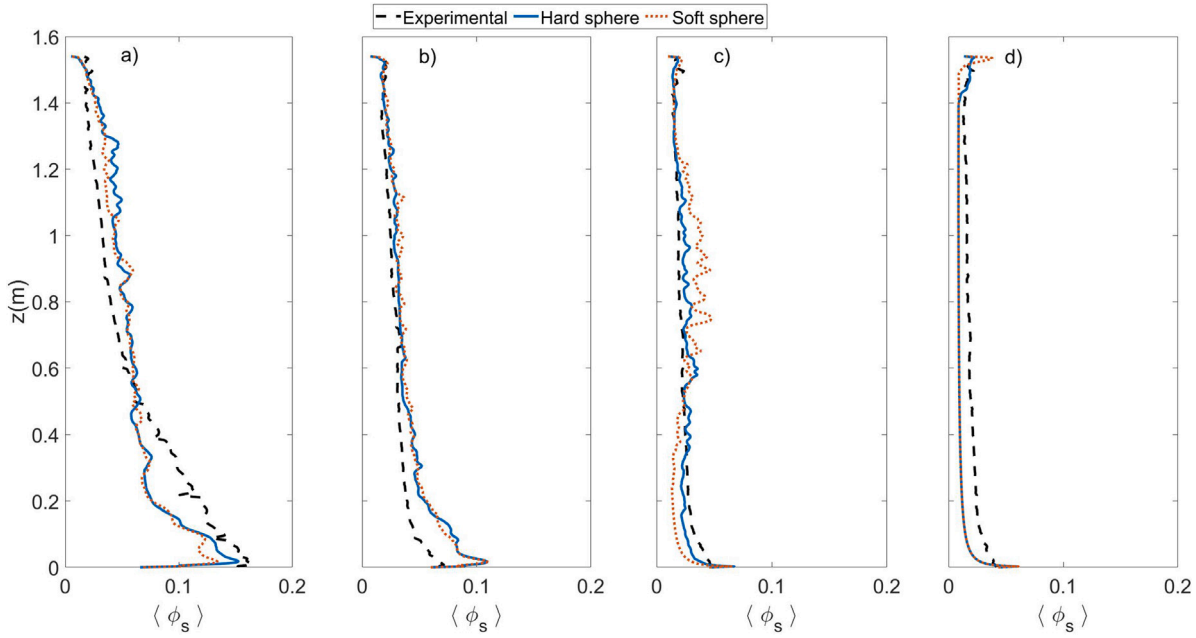

Fig. 3. Axial profiles of time- and laterally-averaged solids holdup. (a) $U_{g,in}$ = 5.55 m/s, (b) $U_{g,in}$ = 5.95 m/s, (c) $U_{g,in}$ = 6.35 m/s, (d) $U_{g,in}$ = 6.74 m/s.

between experiments and CFD-DEM simulations, not only for the gas velocity highlighted in Fig. 2 but for almost the entire gas velocity range. However, it is important to note that there is an under-prediction of the solids fraction at the highest velocity, which corresponds to a condition of almost pneumatic transport. This is a limitation of the drag force formulation that does not perform well under this condition as discussed in Ramírez et al. [19]. However, when comparing collision models, there is a clear overlap between both predictions regardless of the gas velocity. Small differences such as those observed in Fig. 3c, are likely due to insufficient simulation time to fully smooth the average profiles.

Fig. 4 depicts time-averaged radial profiles of the solids fraction, at two different heights within the riser. The first row (Figs. 4a - 4d) corresponds to the bottom of the riser (z = 0.5 m) while the second row (Figs. 4e 4h) represents the top region (z = 1.1 m). Both collision models effectively capture how an increase in gas velocity

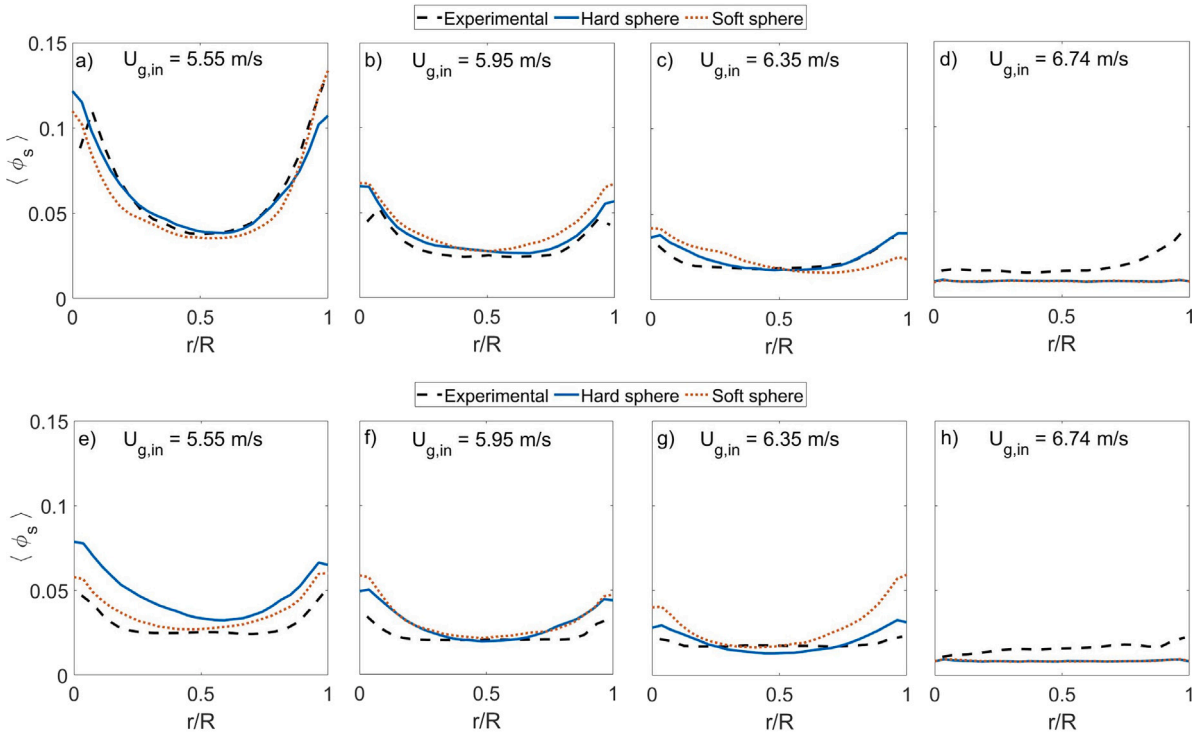

Fig. 4. Radial profiles of time-average solids holdup as a function of the gas superficial velocity. The profiles in bottom section of the riser (z = 0.5 m) are shown in figure a, b, c and d for $U_{g,in}$ = 5.55, 5.95, 6.35 and 6.74 m/s, respectively. The second row shows the profiles at the top section of the riser (z = 1.1 m) in figure e, f, g and h for $U_{g,in}$ = 5.55, 5.95, 6.35 and 6.74 m/s, respectively.

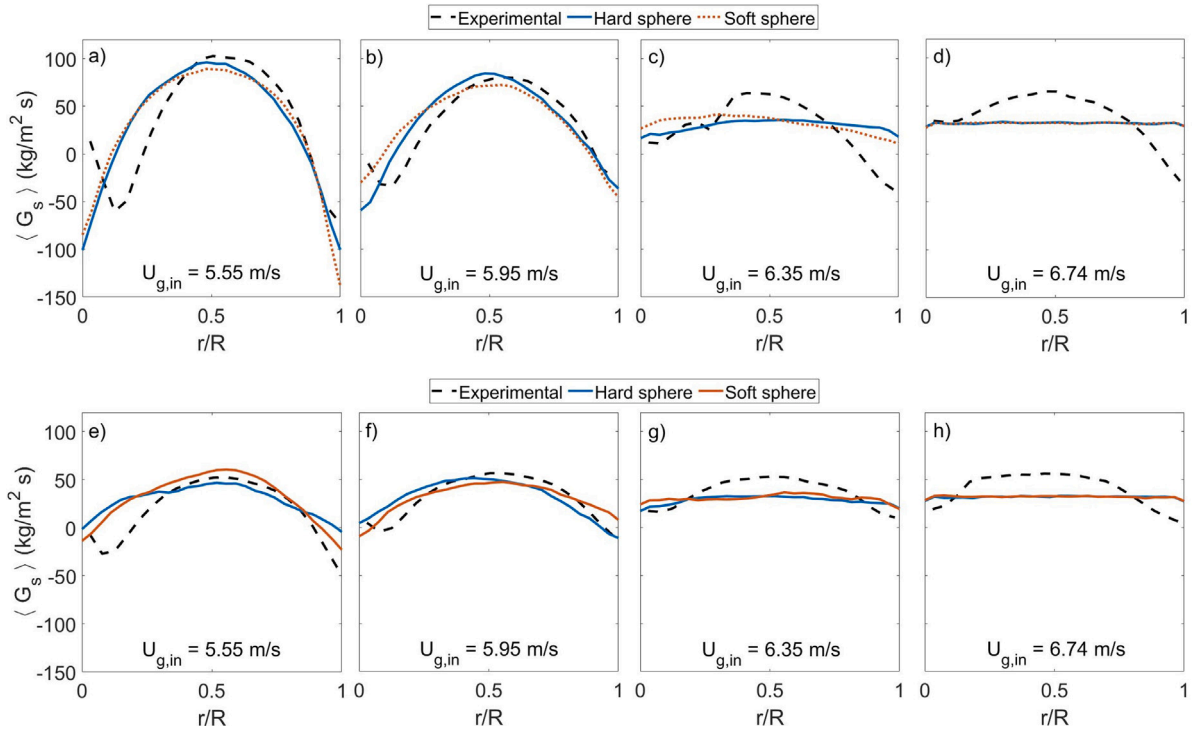

Fig. 5. Radial profiles of time-average solids flux as a function of the gas superficial velocity. The profiles in bottom section of the riser (z = 0.5 m) are shown in figure a, b, c and d for $U_{g,in}$ = 5.55, 5.95, 6.35 and 6.74 m/s, respectively. The second row shows the profiles at the top section of the riser (z = 1.1 m) in figure e, f, g and h for $U_{g,in}$ = 5.55, 5.95, 6.35 and 6.74 m/s, respectively.

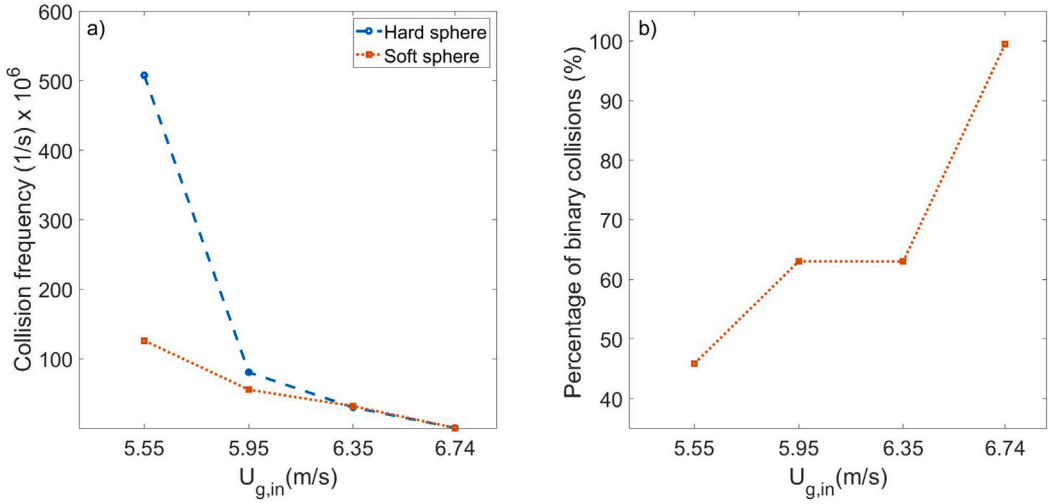

Fig. 6. Behavior of collision variables as a function of the superficial gas velocity. (a) collision frequency, (b) percentage of binary collisions predicted by the soft sphere approach.

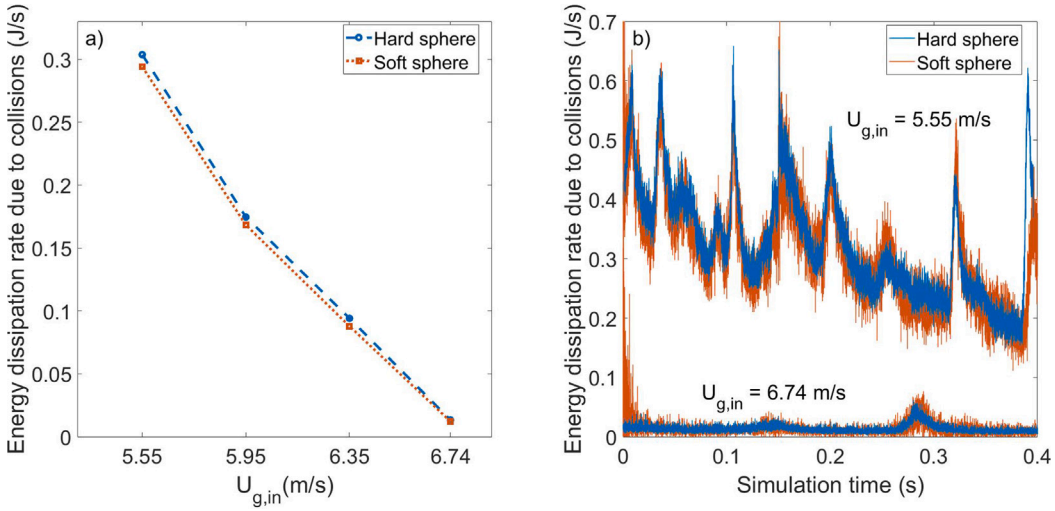

Fig. 7. Behavior of the energy dissipated during collisions. (a) as a function of the superficial gas velocity (b) as a function of time for $U_{g,in}$ = 5.55 and 6.74 m/s.

flattens the radial profiles. The similarity between both collision models persists at the different gas velocities and different sections in the riser. Notably, at the lowest gas velocity in the top section of the riser (Fig. 4e), the hard sphere consistently predicts a higher solid fraction along the radius. This might be a consequence of the low gas velocity value, promoting a higher solids fraction in the riser. Consequently, this could increase collision frequencies, leading to differences between the predictions of both collision approaches. This hypothesis will be thoroughly investigated in the subsequent sections.

Fig. 5 presents a comparative analysis of the time-averaged solids flux for different superficial gas velocities and riser heights, similar to the presentation in Fig. 4. The observations recall the trends found in the radial profiles of solids fractions (Fig. 4); the increase in the superficial gas velocity flattens the radial variations in solids flux. Moreover, there is a high degree of similarity between the predictions of the collision models and these predictions are in line with the experimental behavior. However, two differences appear when comparing the plots in Figs. 4 and 5. Firstly, despite the acceptable accuracy of both collision models predicting the experimental solids fraction at $U_{g,in}$ = 6.35 m/s (Figs. 4c and 4g) the corresponding predictions of solids flux in Figs. 5c and 5g are significantly flatter than in the experiments. This discrepancy, previously noted by Ramirez et al. [19] using only the hard sphere, was attributed to inaccuracies in predicting particles velocities - the other variable involved in the computation of the solids flux. Notably, changing the collision model does not appear to rectify this disparity. Secondly, the discrepancy observed between the two collision models in Fig. 4e is not evident in terms of solids flux in Fig. 5e. This suggests that under these conditions, the collision models might reach slightly different predictions in the particle velocity, resulting in remarkably similar values of solids flux.

The consistent similarities observed in this section regarding solids content distribution between the two collision models are confronted in the section below focusing on collision variables and CPU-performance.

3.2. Collision variables

Fig. 6 presents the behavior of relevant collision variables as a function of the superficial gas velocity. In Fig. 6a, the dependency of collision frequency on superficial gas velocity is depicted using both collision models. The figure illustrates that at higher gas velocities, the collision frequency remains notably similar, with appreciable deviations at $U_{g,in}$ = 5.95 m/s but significant differences at $U_{g,in}$ = 5.55 m/s. This could be explained by the higher solids fraction observed at lower gas velocities, as illustrated in Figs. 3 and 4. Under these dense configurations, particles tend to collide more frequently, which is dampened by the overlap allowed between particles in the soft sphere approach.

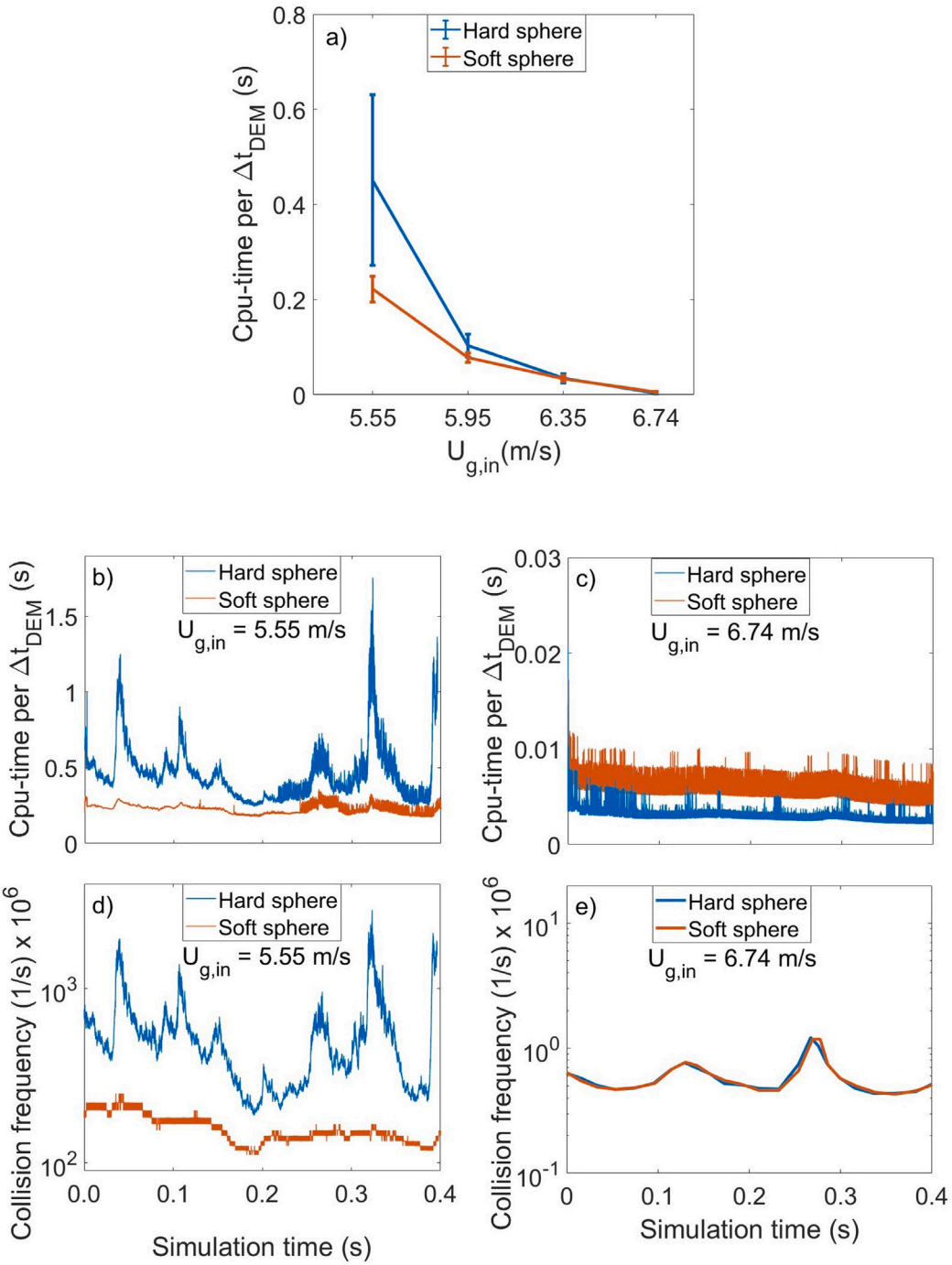

Fig. 8. Relation between CPU-time and collision frequency for both collision models. (a) CPU-time per Δt_{DEM} as a function of the superficial gas velocity, (b) and (c) behavior of cpu-time as a function of time for $U_{g,in}$ = 5.55 and 6.74 m/s, respectively. (d) and (e) behavior of collision frequency as a function of time for $U_{g,in}$ = 5.55 and 6.74 m/s, respectively.

Contrarily, the hard sphere model prohibits overlap of the particles. To support this hypothesis, Fig. 6b presents the average percentage of binary collisions predicted by the soft sphere approach in the riser. Generating a similar plot for the hard sphere is not possible, as it inherently treats any set of multiple collisions occurring simultaneously as a sequence of binary collisions. The plot reveals a decrease in binary collision at lower gas velocities, wherein at the lowest gas velocity less than half of the collisions are binary. This could explain why the differences between both collision models in Fig. 6a are more apparent at lower gas velocities. It is noteworthy that these percentages are highly dependent on the collision parameters, particularly the spring stiffness. The selected values match the commonly accepted criteria of allowing a maximum overlap between particles of 1% of the particle radius (see Table 2).

Fig. 7 presents a comparison between the collision models regarding energy dissipation. In Fig. 7a, despite substantial differences in collision frequency (see Fig. 6a), the energy dissipation rate due to collision remains almost equal regardless of the gas velocity. This suggests that the additional collisions calculated by the hard sphere model likely occur at very low relative particle velocity, resulting in minimal extra energy dissipation.

Fig. 7b presents more detailed information on the energy dissipation throughout the simulation for both the highest and lowest injected gas velocities of this study. The figure displays a significant difference

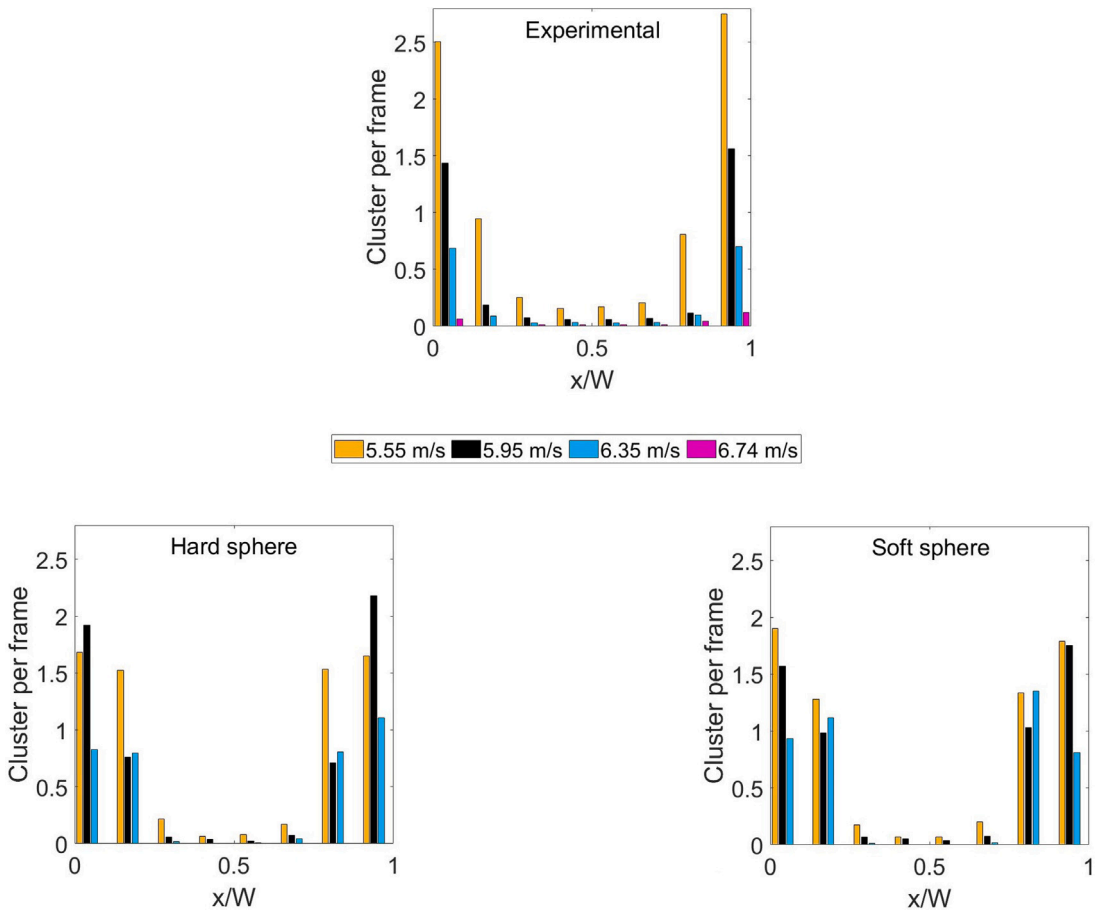

Fig. 9. Cluster frequency as function of the superficial gas velocity.

in predicted energy dissipation between the different gas velocities. Moreover, it reveals more pronounced oscillations in energy dissipation at lower velocities, probably following the dynamics of the formation and breakup of clusters. Finally, the comparison highlights a consistent similarity in energy dissipation between collision models, irrespective of the gas velocity. These similarities in Fig. 7 support the earlier findings in Section 3.1, indicating that differences in collision frequency have a minor effect on the solids distribution within the riser.

The differences in collision frequency between both collision models are expected to manifest in computational time as well, as shown in Fig. 8. In Fig. 8a, the computational time per DEM time step is plotted against injected gas velocity. At higher velocities, both collision models require a similar computational effort. However, notable differences appear at the lowest gas velocity. According to the figure, the hard sphere model on average is more than two times slower than the soft sphere, likely due to the computation of additional collisions (see Fig. 6a). Fig. 8a also shows that not only the mean value of CPU-time but also the standard deviation is affected by the superficial gas velocity in the case of hard sphere model more. Particularly at the lowest velocity, the error bars significantly grow. This large deviation at the lowest velocity is explored in detail in Figs. 8b and 8d. For $U_{g,in}$ = 5.55 m/s, Fig. 8b confirms the larger computational time required by the hard sphere model throughout the simulation. It reveals instances where the hard sphere model can be up to 5–6 times slower than the soft sphere model probably due to the stronger variations in collision frequency.

These profiles of CPU-time have a good correspondence with the collision frequency displayed in Fig. 8d, indicating that peaks in CPU-time for the hard sphere model align with peaks in the computed collision frequency. Furthermore, this comparison highlights the monotonous behavior of the soft sphere approach in terms of CPU-time and collision frequency at lower gas velocities. Contrarily, at higher injected gas velocities (illustrated in Figs. 8c and 8e), different behavior is observed. In this scenario, the hard sphere model exhibits faster computational times throughout the simulation. The hard sphere model is faster along the simulation. Additionally, CPU-time experiences fewer fluctuations, particularly with the results corresponding to the hard sphere model. This could be attributed to reduced cluster formation and a subsequent decrease in collision frequency fluctuations, as shown in Fig. 8e.

3.3. Clustering behavior

Fig. 9 presents the radial distribution of the cluster frequency as a function of the superficial gas velocity. A consistent observation in both experiments and simulations is the tendency of clusters to be predominantly located near the walls. Notably, there is a sharper decrease in the experimental cluster frequency compared to both simulations when moving from the wall toward the center. This discrepancy might arise from bigger clusters formed in the CFD-DEM simulations, independent of the collision model employed. Upon comparing the predictions of the collision models, no relevant differences can be detected, even at the lowest velocity where earlier discussions highlighted significant differences in collision frequency between the models. As discussed prior, the additional (“insignificant”) collisions do not seem to contribute to a decrease in energy dissipation, which is the main driver for cluster formation.

Considering the substantial difference in terms of collision frequency at $U_{g,in}$ = 5.55 m/s, Fig. 10 provides a comparison of the radial distribution of the cluster area under this specific condition. The

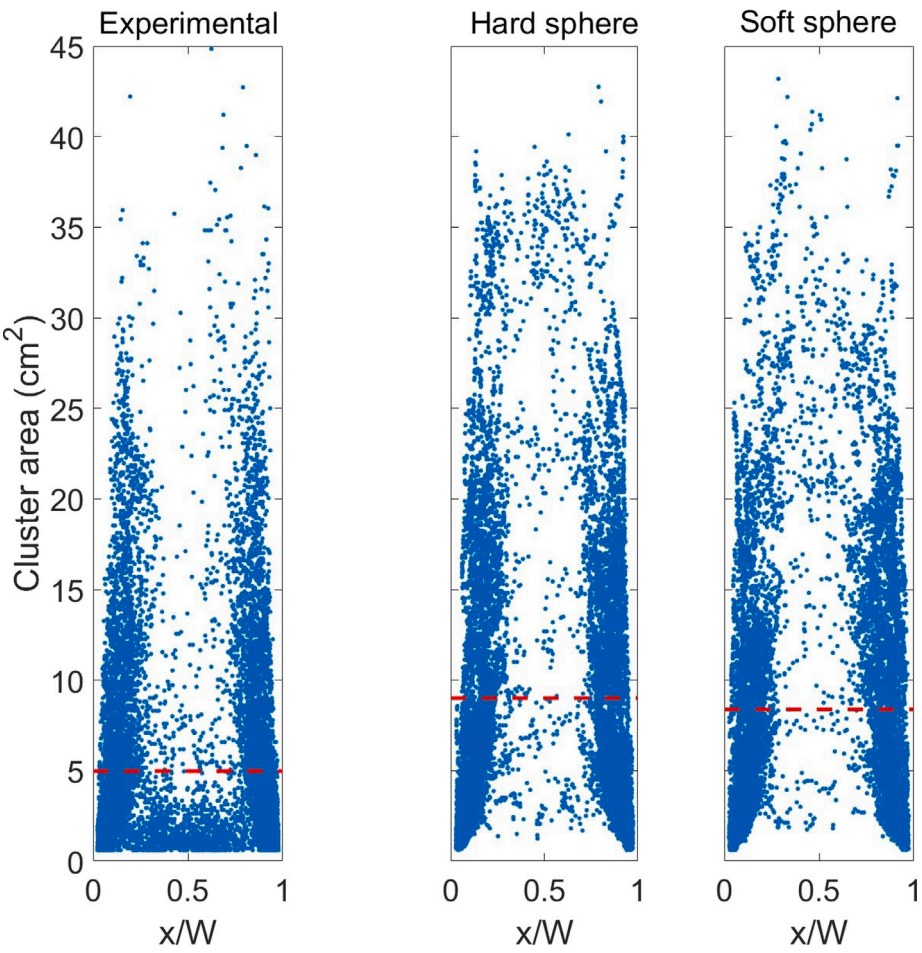

Fig. 10. Cluster area vs. centroid. $U_{g,in}$ = 5.55 m/s. Dotted line represent the average value.

dotted lines represent the average values. Both collision models predict larger clusters on average than those observed in the experiment. Fig. 10 suggests as well a potential explanation. While the experiments detected a high number of small clusters in the core region of the riser (< 5cm^2 near x/W = 0.5), the simulations likely merged these smaller cluster into larger ones near the walls. However, the difference between the collision models is notably smaller, with the clusters predicted by the hard sphere model on average only ~7% larger than those predicted by the soft sphere model.

A similar analysis is conducted concerning the solids holdup, as depicted in Fig. 11. In this figure, we can see that in the experiments the clusters reach a solids holdup that neither of the collision models can reach. This difference could be likely related to the larger clusters predicted by CFD-DEM simulations as shown in Fig. 10. Typically, this additional cluster size corresponds to a dilute region that decreases its average solids holdup. When comparing both collision models, the hard sphere model seems to reach higher maximum values. However, on average, their difference is less than 2%.

4. Conclusions

This study compared the hard sphere and soft sphere collision approaches by evaluating CFD-DEM simulation results of a riser. The evaluation focuses on the predicted hydrodynamics in the fast fluidization regime over a range of superficial gas velocities. Both collision models produce highly similar predictions for the average solids distribution within the riser for all the employed gas velocities. When compared with the experimental behavior, both collision approaches lead to a good match except at the highest velocity. At this extreme value, both collision models predicted a more dilute riser compared to the experimental data.

The evaluation of the collision variables highlighted significant differences in collision frequency and CPU-time. Under high gas velocities approaching the onset of pneumatic transport, the hard sphere model shows faster performance due to the dilute conditions within the riser. However, at lower velocities near the onset of particle carryover, the hard sphere approach exhibits a collision frequency five times higher than the soft sphere approach, resulting in a increased CPU-time demand by 2 to 6 times. This could be a consequence of the fact that the hard sphere model does not allow for overlap between the particles, requiring the computation of all collisions as individual binary interactions, which are more numerous at lower velocities. However, despite the increased number of collisions, their impact on global energy dissipation remains minimal. Moreover, the results indicate that when comparing collision models, the disparity in riser predictions is better explained in terms of energy dissipation rather than collision frequency. Nonetheless, the collision frequency significantly influences computational demand when comparing these models. Future studies could consider existing improvements over the traditional hard or soft sphere approach implemented here, e.g., Lu et al. [21] and Buist et al. [22].

Regarding clustering behavior, despite variations in collision, both collision models predicted a relatively similar formation of clusters. Even at the lowest velocity the differences in size and solids holdup never exceeded 7% and 2%, respectively.

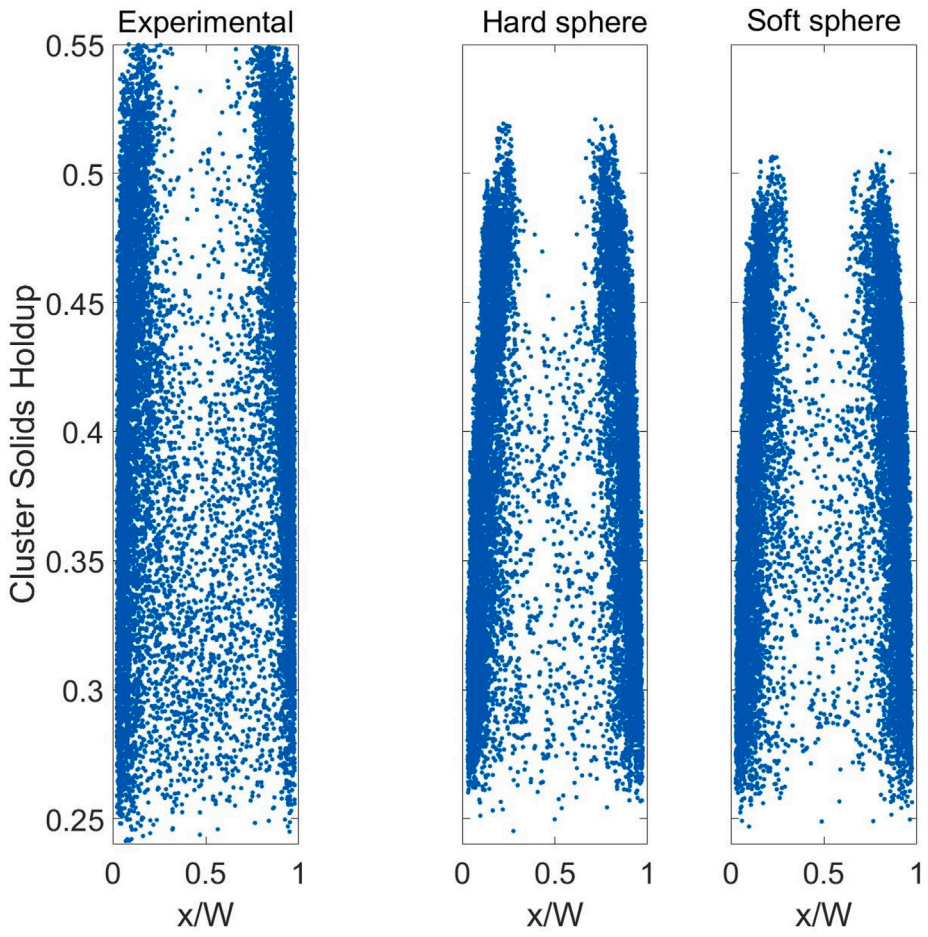

Fig. 11. Cluster solids holdup vs. centroid. $U_{g,in}$ = 5.55 m/s.

CRediT authorship contribution statement

J.G. Ramírez: Writing – original draft, Visualization, Validation, Supervision, Software, Methodology, Investigation, Formal analysis, Data curation, Conceptualization. **Z. Liu:** Visualization, Validation, Formal analysis, Data curation. **M.W. Baltussen:** Writing – review & editing, Software, Investigation, Funding acquisition, Formal analysis, Conceptualization. **K.A. Buist:** Writing – review & editing, Supervision, Methodology, Funding acquisition, Conceptualization. **J.A.M. Kuipers:** Writing – review & editing, Supervision, Software, Resources, Project administration, Funding acquisition, Formal analysis, Conceptualization.

Declaration of Generative AI and AI-assisted technologies in the writing process

During the preparation of this work the authors used ChatGPT in order to improve language and readability. After using this tool, the authors received and edited the content as needed and take full responsibility for the content of the publication.

Declaration of competing interest

The authors declare the following financial interests/personal relationships which may be considered as potential competing interests: J.A.M. Kuipers reports financial support was provided by Dutch Research Council. If there are other authors, they declare that they have no known competing financial interests or personal relationships that could have appeared to influence the work reported in this paper.

Acknowledgments

This work was supported by the Netherlands Center for Multiscale Catalytic Energy Conversion (MCEC), an NWO Gravitation programme funded by the Ministry of Education, Culture and Science of the government of the Netherlands.

This research has received funding from the European Union's Horizon 2020 research and innovation programme under the Marie Skłodowska-Curie grant agreement No 801359.

Data availability

Data will be made available on request.

References

[1] B.P.B. Hoomans, Granular Dynamics of Gas-Sold Two-Phase Flows (Ph.D. thesis), Universiteit Twente, 2000.

[2] J.W. Chew, R. Hays, J.G. Findlay, T.M. Knowlton, S.B.R. Karri, R.A. Cocco, C.M. Hrenya, Cluster characteristics of geldart group b particles in a pilot-scale CFB riser. I. monodisperse systems, Chem. Eng. Sci. 68 (2012) 72–81, http://dx.doi.org/10.1016/j.ces.2011.09.012.

[3] T. Tanaka, S. Yonemura, K. Kiribayashi, Y. Tsuji, Cluster formation and particle-induced instability in gas-solid flows predicted by the DSMC method, J. SME Int. J. Ser. B 39 (1996) 239–245, http://dx.doi.org/10.1299/jsmeb.39.239.

[4] M.T. Shah, R.P. Utikar, V.K. Pareek, G.M. Evans, J.B. Joshi, Computational fluid dynamic modelling of FCC riser: A review, Chem. Eng. Res. Des. 111 (2016) 403–448, http://dx.doi.org/10.1016/j.cherd.2016.04.017.

[5] E. Helland, H. Bournot, R. Occelli, L. Tadrist, Drag reduction and cluster formation in a circulating fluidised bed, Chem. Eng. Sci. 62 (2007) 148–158, http://dx.doi.org/10.1016/j.ces.2006.08.012.

[6] G.J. Heynderickx, A.K. Das, J.D. Wilde, G.B. Marin, Effect of clustering on gas-solid drag in dilute two-phase flow, Ind. Eng. Chem. Res. 43 (2004) 4635–4646, http://dx.doi.org/10.1021/ie034122m.

[7] J. Xu, J.X. Zhu, Visualization of particle aggregation and effects of particle properties on cluster characteristics in a CFB riser, Chem. Eng. J. 168 (2011) 376–389, http://dx.doi.org/10.1016/j.cej.2011.01.044.

[8] X. Lan, X. Shi, Y. Zhang, Y. Wang, C. Xu, J. Gao, Solids back-mixing behavior and effect of the mesoscale structure in CFB risers, Ind. Eng. Chem. Res. 52 (2013) 11888–11896, http://dx.doi.org/10.1021/ie3034448.

[9] L. Mu, K.A. Buist, J.A.M. Kuipers, N.G. Deen, CFD-DEM simulations of riser geometry effect and cluster phenomena, Adv. Powder Technol. 32 (2021) 3234–3247, http://dx.doi.org/10.1016/j.apt.2021.07.007.

[10] Y. Tsuji, T. Tanaka, S. Yonemura, Cluster patterns in circulating fluidized beds predicted by numerical simulation (discrete particle model versus two-fluid model), Powder Technol. 95 (1998) 254–264.

[11] T. Wang, Y. He, S. Yan, T. Tang, H.I. Schlaberg, Cluster granular temperature and rotational characteristic analysis of a binary mixture of particles in a gas-solid riser by mutative smagorinsky constant SGS model, Powder Technol. 286 (2015) 73–83, http://dx.doi.org/10.1016/j.powtec.2015.08.009.

[12] S. Wang, X. Li, H. Lu, L. Yu, J. Ding, Z. Yang, DSMC prediction of granular temperatures of clusters and dispersed particles in a riser, Powder Technol. 192 (2009) 225–233, http://dx.doi.org/10.1016/j.powtec.2009.01.008.

[13] A.B. Morris, A hybrid DSMC and discrete element modeling approach for particle flows that span dilute to dense regimes, AIP Conf. Proc. 2132 (1) (2019) 070004, http://dx.doi.org/10.1063/1.5119558.

[14] A.E.C. Varas, E.A.J.F. Peters, J.A.M. Kuipers, CFD-DEM simulations and experimental validation of clustering phenomena and riser hydrodynamics, Chem. Eng. Sci. 169 (2017) 246–258, http://dx.doi.org/10.1016/j.ces.2016.08.030.

[15] T. Wang, S. Wang, Y. Shen, Particle-scale study of gas-solid flows in a bubbling fluidised bed: Effect of drag force and collision models, Powder Technol. 384 (2021) 353–367, http://dx.doi.org/10.1016/j.powtec.2021.02.034.

[16] A.E.C. Varas, E.A.J.F. Peters, J.A.M. Kuipers, Experimental study of full field riser hydrodynamics by PIV/DIA coupling, Powder Technol. 313 (2017) 402–416, http://dx.doi.org/10.1016/j.powtec.2017.01.055.

[17] B.P.B. Hoomans, J.A.M. Kuipers, W.J. Briels, W.P.M. van Swaaij, Discrete particle simulation of bubble and slug formation in a two-dimensional gas-fluidised bed: A hard-sphere approach, Chem. Eng. Sci. 51 (1) (1996) 99–118, http://dx.doi.org/10.1016/0009-2509(95)00271-5, URL https://www.sciencedirect.com/science/article/pii/0009250995002715.

[18] N.G. Deen, S.H. Kriebitzsch, M.A. van der Hoef, J.A.M. Kuipers, Direct numerical simulation of flow and heat transfer in dense fluid-particle systems, Chem. Eng. Sci. 81 (2012) 329–344, http://dx.doi.org/10.1016/j.ces.2012.06.055.

[19] J. Ramírez, M.J.A. de Munck, Z. Liu, D.R. Rieder, M.W. Baltussen, K.A. Buist, J.A.M. Kuipers, CFD-DEM evaluation of the clustering behavior in a riser the effect of the drag force model, Ind. Eng. Chem. Res. (2023) http://dx.doi.org/10.1021/acs.iecr.3c00853.

[20] N.G. Deen, M. Van Sint Annaland, M.A. Van der Hoef, J.A.M. Kuipers, Review of discrete particle modeling of fluidized beds, Chem. Eng. Sci. 62 (2007) 28–44, http://dx.doi.org/10.1016/j.ces.2006.08.014.

[21] L. Lu, S. Benyahia, T. Li, An efficient and reliable predictive method for fluidized bed simulation, AIChE J. 63 (12) (2017) 5320–5334, http://dx.doi.org/10.1002/aic.15832, URL https://aiche.onlinelibrary.wiley.com/doi/abs/10.1002/aic.15832.

[22] K. Buist, L. Seelen, N. Deen, J. Padding, J. Kuipers, On an efficient hybrid soft and hard sphere collision integration scheme for dem, Chem. Eng. Sci. 153 (2016) 363–373, http://dx.doi.org/10.1016/j.ces.2016.07.030, URL https://www.sciencedirect.com/science/article/pii/S0009250916304043.